VII. Supporting Research and Technology

ADVANCED ENGINEERING

A. 30-ft-diam Reflector Upgrade Study,

M. S. Katow

1. Introduction

As described previously (SPS 37-52, Vol. II, p. 86), the distortions of an az-el type of antenna resulting from the change in direction of the gravity force due to elevation angle rotation can be resolved from two loading cases. The first is the gravity loading along the symmetric axis, and the other loading is at right angle to the symmetric axis or the antisymmetric direction. The final distortion number is the vector sum of the deflections resulting from the change in the two loadings components.

For an arrangement using radial trusses, the minimum distortion of the reflector is attained if the trusses are arranged so that (1) in the symmetric loading case the deflections are symmetrical about the axis of symmetry, and the ribs deflect to a parabolic curve of longer focal length, and (2) for the antisymmetric case the rib trusses must be deep enough to minimize the deflections from the antisymmetric loading.

To satisfy requirements in (1) easily, without regard to other considerations (such as the effects by wind loading on the driving torques) the truly axially symmetric rigid truss arrangement, with structure to mask out the reaction effects of the unsymmetric elevation bearings, is the ideal solution.

The two elevation bearings cause non-symmetric deflections, and there is a need for passive compensating devices, such as springs, to reduce the symmetric distortion without interacting and increasing the distortion in the antisymmetric loading case.

This article describes the result of adding a spring-type passive compensating device to the non-axial symmetric 30-ft reflector structure at the Venus DSS. Only the results of the analytical study using a structural computing program (NASTRAN) are presented.

2. Discussion

Figure 1 shows in schematic the arrangement of the trusses in the tipping assembly. The reflector structure

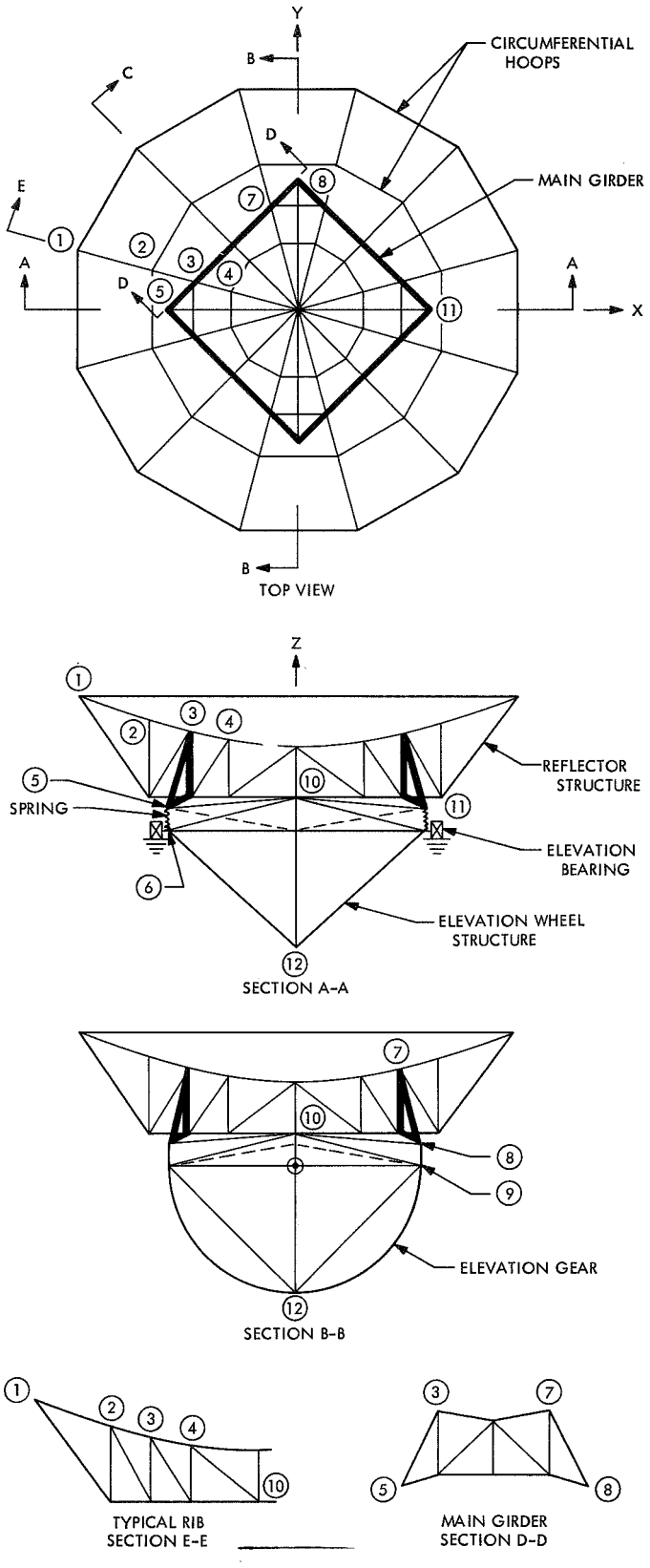

Fig. 1. Truss arrangements of tipping assembly in 30-ft-diam-antenna

consists of radial rib trusses and circumferential loop trusses supported by the main girder and the central connection to the elevation wheel structure at node 10. The main girder support points are, typically, nodes 5 and 8 of the elevation wheel structure.

For clarity purposes, the diagonals in the upper surface of the reflector structure are not shown. The quadripod is also deleted, since it is now supported from the elevation wheel structure and has little or no effect on the reflector distortion. The tipping assembly is supported on the two elevation bearings, and the pinion gear is anchored to the yoke, which is also not shown because of the unrestrained supporting arrangement.

Presently, the main girder is rigidly supported in the Z direction by solid bar members between nodes 5 and 6 plus 8 and 9 as well as by bars on the other reflector half. Because of the high stiffness of node 6 as compared to node 8, the main girder, and consequently the reflector

CONTOUR DEFINITIONS

LABEL	NORMAL ERROR, in.
A	-0.035
B	-0.030
C	-0.025
D	-0.020
E	-0.015
F	-0.010
G	-0.005
H	0.000
I	0.005
J	0.010
K	0.015
L	0.020
M	0.025
N	0.030
O	0.035

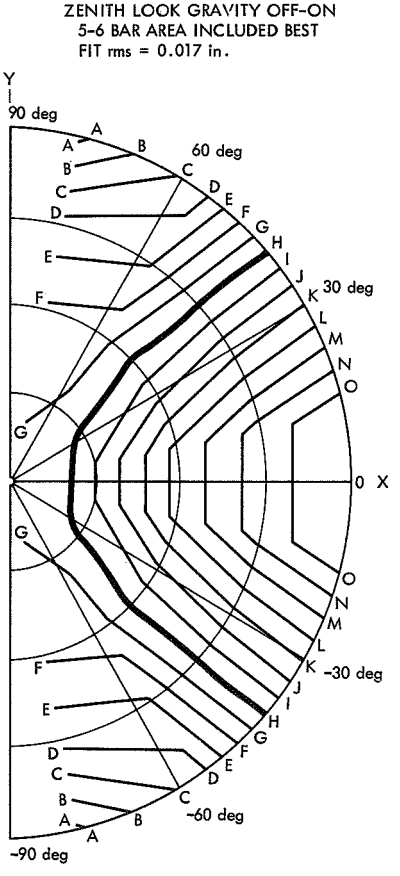

Fig. 2. Deflection contour map for zenith look for half dish, 30-ft-diam-antenna, best fit rms = 0.017 in.

structure, deflects non-uniformly about the plane of symmetry (Y-Z) for zenith-look gravity load. The resulting best-fit deflections are shown in Fig. 2, with the rms value of 0.017 in.

By replacing the 5–6 bar (17$\frac{3}{16}$ in. long) with a spring that deflects 0.026 in. for a 900-lb load, the Z deflection of node 5 can approach that of node 8 resulting in a more symmetrically shaped deflection pattern. After best-fit, the deflection pattern is shown in Fig. 3 with the resulting reduction of the rms to 0.002 in.

Although the addition of the spring improved the gravity-deflection patterns, the reflector structure became more sensitive to distortion from wind loading. Additional wind bracing connecting nodes 5, 10, 11 and a sliding connection in Z direction to node 12 may be required. This bracing will greatly increase the stiffness of the reflector structure in the X–Z plane and a sliding connection to node 12 will be necessary only if RF boresight pointing accuracy is involved.

3. Conclusions

The 30-ft reflector structure is a practical design, using rigid bars that can be improved for gravity distortion by the addition of passive compensators in a form of springs. However, additional bracing for minimizing distortions due to wind loadings may be desirable.

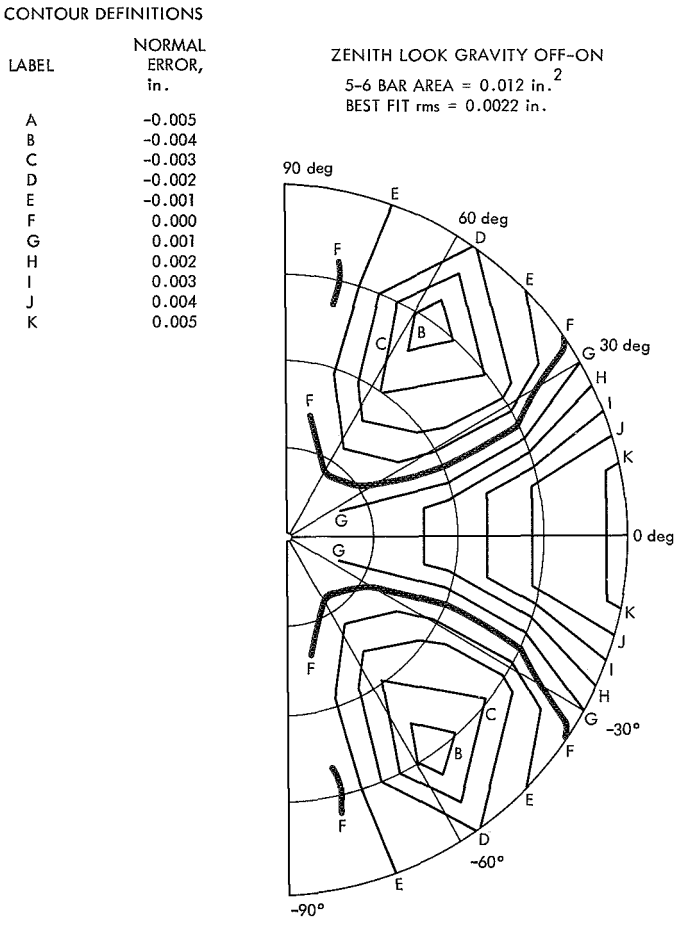

Fig. 3. Deflection contour map for zenith look, half dish, best fit rms = 0.002 in.

B. A Method for Selecting Antenna Rigging Angles to Improve Performance, *R. Levy*

1. Introduction

Methods to reduce root-mean-square (rms) deviations for antenna reflector surfaces are of great interest because of the unfavorable influence of large deviations upon the antenna's RF performance. By convention, these deviations are determined with respect to the best-fitting paraboloid by means of a mathematical procedure (Ref. 1) that permits rigid body motions of the reflector and a change in focal length. From an RF standpoint, the change in the paraboloidal configuration that is implied by the best-fit parameters[1] is either not objectionable or can be compensated with physical adjustment.

One major source of reflector distortion is the change in deflections caused by gravity as the antenna is moved over a range of elevation positions. This is the result of the relative change in direction of gravity loading (weight of structure and components) with respect to the structure.

[1]There can be up to six parameters consisting of three translations, two rotations, and one change in focal length.

2. Antenna Rigging to Reduce rms Deviations

A common field procedure that is used to reduce the extreme rms deviations is to adjust the surface as closely as possible to the exact paraboloid with the antenna positioned at some intermediate (rigging) angle. When this is done, the gravity distortions at the horizon and zenith positions are substantially reduced because these now are the result of only the change in loading from the rigging angle position. A good choice is to pick the rigging angle that causes the horizon and zenith rms deviations to be equal. It appears that this will provide the smallest peak rms deviation over the entire attitude range. Another, and possibly superior, choice is to select the rigging angle that minimizes an average weighted rms deviation over the entire elevation range. A logical weighting function for this would be based upon the relative importance of the surface accuracy at each elevation angle.

Usually, rigging angles have been selected by either of two procedures:

(1) By an arbitrary choice, say of 45 deg. This has the disadvantage that a poor guess will result in higher-than-necessary surface deviations.

(2) As the result of a parameter study using the analytic predictions for deviations. The study is performed by first assuming a trial rigging angle and then computing the best-fit rms deviations at the horizon attitude and at the zenith attitude. The trial rigging angle is incremented and the process is repeated until a sequence of extreme rms values is generated for a discrete set of trial angles. The selection is made from inspection of these values. This method is cumbersome and has the disadvantage of a large number of computations needed to best-fit each of the distortion vectors for every trial rigging angle. If weighted-average minimization is to be performed, the number of best-fit computations becomes excessive because of the necessity to compute the rms at elevations intermediate to the zenith and horizon attitudes.

3. Equations for Closed-Form Computations

A convenient method can be used to determine the best-fit rms distortions at any elevation attitude. This will facilitate a parameter study for determination of the rigging angle that minimizes the weighted-average rms. If alternatively, the objective is to make the rms at zenith equal to the rms at the horizon, the rigging angle can be obtained immediately by direct computation, thereby replacing the need to perform a parameter study. A major advantage of the approach to be described is that instead of performing the best-fit computations repeatedly with each incremental choice of rigging angle, these computations are executed once only for each of the two following vectors consisting of the cartesian components of the displacements at a prescribed set of reflector surface nodes:

$\{u_y\}$ = displacement vector for gravity loading applied parallel to the reflector y-axis (in a vertical plane when the antenna points to horizon)

$\{u_z\}$ = displacement vector for gravity loading applied parallel to the reflector z-axis (in a vertical plane when the antenna points to the zenith)

The assumption of the linearity of loading and displacements frequently permits great simplification in the conventional parameter study. The assumption will be made here also, and it follows from this that the displacements at any elevation attitude angle α are linear combinations of $\{u_y\}$ and $\{u_z\}$.

Thus,

$$\{u\} = \eta\{u_y\} + \zeta\{u_z\} \tag{1}$$

where

$$\left.\begin{aligned} \eta &= \cos\gamma - \cos\alpha \\ \zeta &= \sin\gamma - \sin\alpha \end{aligned}\right\} \tag{2}$$

and γ is the rigging angle.

Since the coefficients in Eq. (2) reflect the changes from the rigging position, Eq. (1) represents the change in distortion from the rigging position. Figure 1 shows the orientation of the coordinate system at the elevation angle α and the components of the gravity loading w.

For the computation of the rms best-fit rms surface deviations (SPS 37-40, Vol. IV, pp. 176–186), the vector of half pathlength RF deviations could be expressed as

$$\{\rho\} = [A]\{u\} + [B]\{h\} \tag{3}$$

where $[A]$ and $[B]$ are geometry matrices containing invariant data that depends only upon the coordinates of the reflector surfaces nodes, and $\{h\}$ is the 6×1 vector of the best-fit parameters.

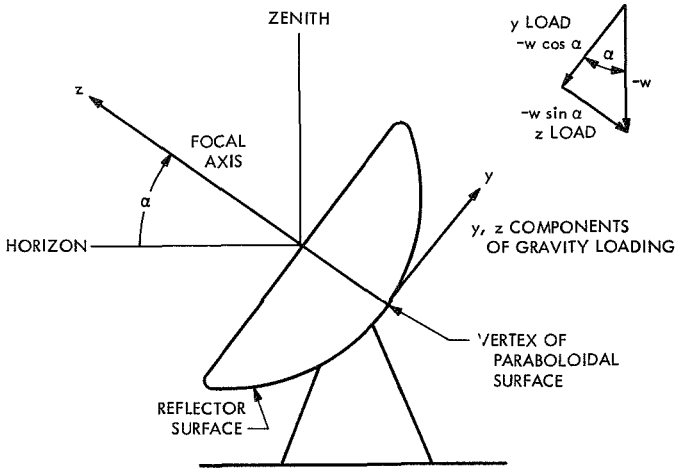

Fig. 1. Coordinate system for reflector

Forming the sums of squares, e.g., $\{\rho\}^t\{\rho\}$, and taking the partial derivatives with respect to $\{h\}$ results in the following solution for the best-fit parameters:

$$\{h\} = -[B^tB]^{-1}[B]^t[A]\{u\} \tag{4}$$

Substituting Eq. (4) in Eq. (3),

$$\{\rho\} = [R]\{u\} \tag{5}$$

in which

$$[R] = ([A] - [B][B^tB]^{-1}[B]^t[A]) \tag{6}$$

Then, substituting Eq. (1) in Eq. (5),

$$\{\rho\} = [R][u_y u_z]\begin{Bmatrix}\eta\\ \zeta\end{Bmatrix} \tag{7}$$

Forming the sums of squares,

$$\{\rho\}^t\{\rho\} = \eta^2(u_y^tR^tRu_y) + \zeta^2(u_z^tR^tRu_z) + 2\eta\zeta(u_y^tR^tRu_z) \tag{8}$$

Let

SS_y = sums of squares of half pathlength deviation for y-loading

SS_z = sums of squares of half pathlength deviation for z-loading

$\{\rho_y\}, \{\rho_z\}$ = corresponding half pathlength deviation vectors

Then

$$\{\rho\}^t\{\rho\} = \eta^2SS_y + \zeta^2SS_z + 2\eta\zeta\{\rho_y\}^t\{\rho_z\} \tag{9}$$

To make the sums of squares equal in the zenith and horizon attitudes, substitute the following in Eq. (9):

$$\left.\begin{array}{lll}\text{Zenith:} & \eta = \cos\gamma, & \zeta = \sin\gamma - 1\\ \text{Horizon:} & \eta = \cos\gamma - 1, & \zeta = \sin\gamma\end{array}\right\} \tag{10}$$

and then equate the zenith and horizon sums of squares. After canceling and rearranging terms, the following equation is obtained:

$$(2SS_y - 2\{\rho_y\}^t\{\rho_z\})\cos\gamma - (2SS_z - 2\{\rho_y\}^t\{\rho_z\})\sin\gamma = SS_y - SS_z \tag{11}$$

Equation (11) is of the form

$$A\cos\gamma - B\sin\gamma = C \tag{12}$$

where

$$A = 2SS_y - 2\{\rho_y\}^t\{\rho_z\} \tag{12a}$$

$$B = 2SS_z - 2\{\rho_y\}^t\{\rho_z\} \tag{12b}$$

$$C = SS_y - SS_z \tag{12c}$$

The solution of Eq. (11) for the desired rigging angle is

$$\gamma = \phi - \epsilon \tag{13}$$

where

$$\epsilon = \tan^{-1}\left(\frac{B}{A}\right) \tag{14a}$$

$$\phi = \cos^{-1}\left(\frac{C}{[A^2 + B^2]^{1/2}}\right) \tag{14b}$$

Hence, to compute the optimum rigging angle, it is necessary only to know the sums of the squares of the deviation vectors (which can be computed from the best-fit rms deviations) for both y-loads and z-loads acting alone and also to save the corresponding deviation vectors to compute the sum of the cross products. All of these quantities are readily available from the best-fit computation program. After the rigging angle has been

found, Eq. (9) in conjunction with Eq. (2) can be used to compute the sums of squares at any attitude, which leads immediately to the corresponding rms deviations.

4. Example 1

The rigging angle will be computed to obtain equal rms distortions at zenith and horizon for the 210-ft-diameter antenna. The following data is available (SPS 37-52, Vol. II, pp. 86–92) from existing computations based upon an arbitrarily chosen rigging angle of 45 deg:

Attitude	RMS deviation, in.
Zenith	0.075
Horizon	0.040

The analysis of this antenna assumed symmetry about the y–z and the x–z planes. As a result, it follows that

$$\{\rho_y\}^t \{\rho_z\} = 0$$

Although SS_y and SS_z were not given, Eq. (9) can be used to find SS_y/N and SS_z/N (N = number of surface points) as follows:

$$\text{Zenith:} \quad (0.075)^2 = (0.7071)^2 \frac{SS_y}{N} + (-0.2929)^2 \frac{SS_z}{N}$$

$$\text{Horizon:} \quad (0.040)^2 = (-0.2929)^2 \frac{SS_y}{N} + (0.7071)^2 \frac{SS_z}{N}$$

Solving these equations simultaneously provides

$$\frac{SS_y}{N} = 110.81 \times 10^{-4}$$

$$\frac{SS_z}{N} = 12.98 \times 10^{-4}$$

From Eqs. (12a), (12b), (12c),

$$\frac{A}{N} = 221{,}62 \times 10^{-4}$$

$$\frac{B}{N} = 25.96 \times 10^{-4}$$

$$\frac{C}{N} = 97.83 \times 10^{-4}$$

From Eqs. (14a), (14b),

$$\epsilon = 6°41'$$

$$\phi = 64°00'$$

and from Eq. (13), the desired rigging angle is

$$\gamma = 57°19'$$

Finally, straightforward substitution in Eq. (10) and then Eq. (9) yields, for either zenith or horizon attitudes,

$$\frac{SS}{N} = 32.61 \times 10^{-4}$$

or

$$\text{rms deviation} = 0.0571 \text{ in.}$$

The relative reduction in the maximum peak rms at the computed rigging angle with respect to the previous maximum, which occurred at the zenith position, for the arbitrary 45-deg rigging angle is

$$\text{reduction in maximum peak} = \frac{0.075 - 0.057}{0.075} \times 100\%$$

$$= 24\%$$

On the other hand, the increase of the previous minimum peak rms, which occurred at the horizon position, is

$$\text{increase in minimum peak} = \frac{0.040 - 0.057}{0.040} \times 100\%$$

$$= 42\%$$

This example illustrates the effectiveness of the present approach when the constraint is with respect to the maximum rms at any elevation attitude. Here the maximum peak that occurred at the zenith end of the elevation range was reduced at the expense of an increase at the horizon end of the range. The design for an alternative constraint, which entails a weighting function of the elevation attitude, is illustrated in the following example.

5. Example 2

Surface distortions for an 85-ft-diameter antenna that had been determined previously (SPS 37-52, Vol. II,

pp. 99–105) were used again as input to the best-fit rms computer program. This time, new instructions were provided to develop the necessary additional terms and perform the computations to find the rigging angle for equal rms at zenith and horizon.

The results obtained for this antenna, which were based upon 115 surface nodes distributed over one-half of the (symmetrical) structure, are given in Table 1. The maximum values of the best-fit rms surface distortions are compared for: (1) an arbitrary choice of rigging angle; (2) the rigging angle that is presently used for the antenna (found by an approximated parameter study); and (3) the rigging angle computed by the methods presented here. Table 1 shows that the minimum error is achieved with the rigging angle computed according to the proposed new method.

Table 1. Comparison of best-fit rms deviations for various rigging angles

Rigging angle, deg	Method	Best-fit rms half pathlength error, in.		Extreme rms error, in.	Reduction of extreme rms error, %
		Horizon	Zenith		
45.0	Arbitrary choice	0.0247	0.0146	0.0247	Basic
40.0	Parameter study	0.0228	0.0161	0.0228	7.7
31.3	Eq. (13)	0.0189	0.0189	0.0189	23.5

Finally, a parameter study was performed for this antenna to find the rigging angle for a weighted-average rms minimization. The two sums of squares and the cross product term [see Eq. (9)] developed by the best-fit program were used in a separate *Fortran* program that performed the computations. The weighting function was equal to the cosine of the elevation attitude angle. This provides the minimum expected value of the rms deviation for targets uniformly distributed with respect to elevation angles between zenith and horizon. Rigging angles and elevation angles in the study were incremented by 5 deg from horizon to zenith. For each rigging angle, the weighted rms deviations were computed for the complete set of elevation attitude angles. It was found to within four significant figures that rigging angles of either 25 or 30 deg were optimal. The corresponding weighted rms deviations are plotted in Fig. 2. The computer program to perform the parameter study required less than 7 sec of computer time on the Univac 1108.

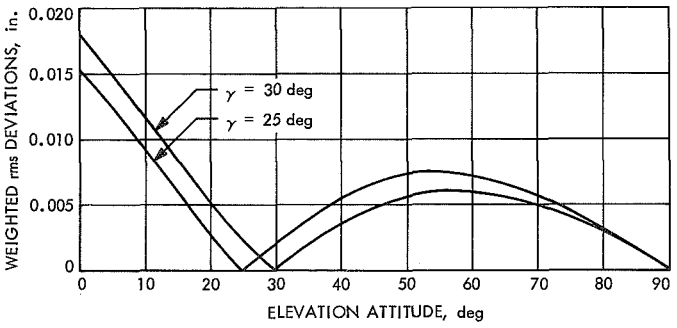

Fig. 2. RMS deviations weighted by cos α

6. Conclusions

A new procedure is described to compute the reflector surface rms gravity distortions from the best-fitting paraboloid at any arbitrary antenna elevation attitude. To apply the procedure, it is necessary to know the vectors of half pathlength deviations from the best-fitting paraboloids for two independent gravity loadings. Once these two vectors are known, no further best-fitting computations are performed for any arbitrary elevation attitudes where the best-fit rms distortion is to be determined. The simplicity with which the rms distortions can be computed for arbitrary elevation angles facilitates the selection of the optimum rigging angle to minimize gravity distortions. In the case where it is desired to achieve the minimum rms distortion over the entire elevation range, the optimum rigging angle can be obtained by a closed-form computation from the equation presented. In the case where it is desired to minimize the weighted-average rms distortion over a given elevation attitude range, the parameter study necessary to choose the best rigging angle is facilitated by the rapidity with which the rms distortions can be computed.

Reference

1. Katow, M. S., and Schmele, L., *UTKU/Schmele Parabaloid RMS Best-Fit Program, Volume I*, Technical Report 32-979. Jet Propulsion Laboratory, Pasadena, Calif., Apr. 15, 1970.

C. Low-Frequency Low-Level Stress Reversals on an Assembly of Bolted Joint Specimens,

V. B. Lobb

1. Introduction

JPL is currently using an inorganic zinc coating as an effective corrosion barrier on the 210-ft-diam antennas. This coating exhibits excellent corrosion protection and a high frictional coefficient for static loads. However, on previous joint integrity research (SPS 37-52, Vol. II) JPL found that the inorganic zinc coating broke down on the contact surfaces when undergoing stress reversal. Once this breakdown occurs, there is an appreciable loss in bolt preload and joint slip results. This breakdown occurred at a 20,000-psi (design allowable) net section stress level.

To ensure that this desirable coating could be used without joint slippage, JPL needed to know the exact stress level at which this coating breakdown would occur. A research program was initiated to further study bolted structural assemblies with plain mill-scale faying surfaces and inorganic zinc paint faying surfaces. Plain mill scale was assigned the role of a control surface by which the inorganic zinc painted surface was to be compared. A series of different design stress levels was used to determine or bracket the desired breakdown point.

Previous tests had already demonstrated the ability of the inorganic zinc paint surface to resist slip displacement under static loading. This research was directed toward short-term, relatively low-level repetitive load reversals. This research investigated the effect of surface conditions, bolt design, bolt strength level, and applied stress versus joint-slip displacement. The objective was to determine which design parameter and what stress level would affect inorganic zinc-painted coatings on bolted connections.

2. Research Program

A series of low-frequency, low-level stress reversal tests was conducted on assemblies of bolted-joint specimens. The test series consisted of 116 separate scheduled tests conducted on 58 specimens. The tests were conducted in a special H-frame test stand which alternately reversed specimen load to a given percent of design allowable. Load was maintained within an accuracy of $\pm$ 5%. Slip displacement was measured on both sides of the specimen to a sensitivity of 0.0001 of an inch. Dial-indicating gauges mounted on the specimens for the duration of the test were employed.

The test evaluated three parameters as they influenced joint behavior under complete reversal of load. These parameters are as follows:

(1) Four bolt types: ASTM A325, ASTM A490, hexagon-structural, and interference-body-bearing bolts.

(2) Two faying surface conditions: dry mill scale and inorganic zinc paint.

(3) Plate stresses: 25%, 37½%, 50%, 62½%, 75%, and 87½% of design allowable net section stresses.

Parameters which remained constant for all tests included the following:

(1) All joints were two-bolt single shear connections.

(2) All joint material was ASTM A36 steel.

(3) Each joint was made of a hot-rolled steel angle which was connected to a hot-rolled steel gusset plate.

(4) All bolts were ¾ 10 UNC.

(5) All bolts were tightened in accordance with a turn-of-the-nut installation procedure.

(6) All A325 bolts were assembled with one washer under the nut.

(7) All A490 bolts were assembled with washers under both the nut and the head.

(8) All bolts, nuts, and washers were in the as-received black-finished condition.

(9) All the joint geometry, allowable stresses, and design procedures followed the recommendations of the American Institute of Steel Construction.

3. Test Procedure

Testing was performed in a 200,000-lb capacity Enerpac H-frame hydraulically operated press (Fig. 1). Special coupling fixtures were employed, which permitted both tension and compression loads to be applied to the specimen without removing it from the press for the duration of the test.

Each specimen was installed in a series with a strain gauge load transducer used to monitor load for the duration of the test. Two sets of dual dial-indicating gauges

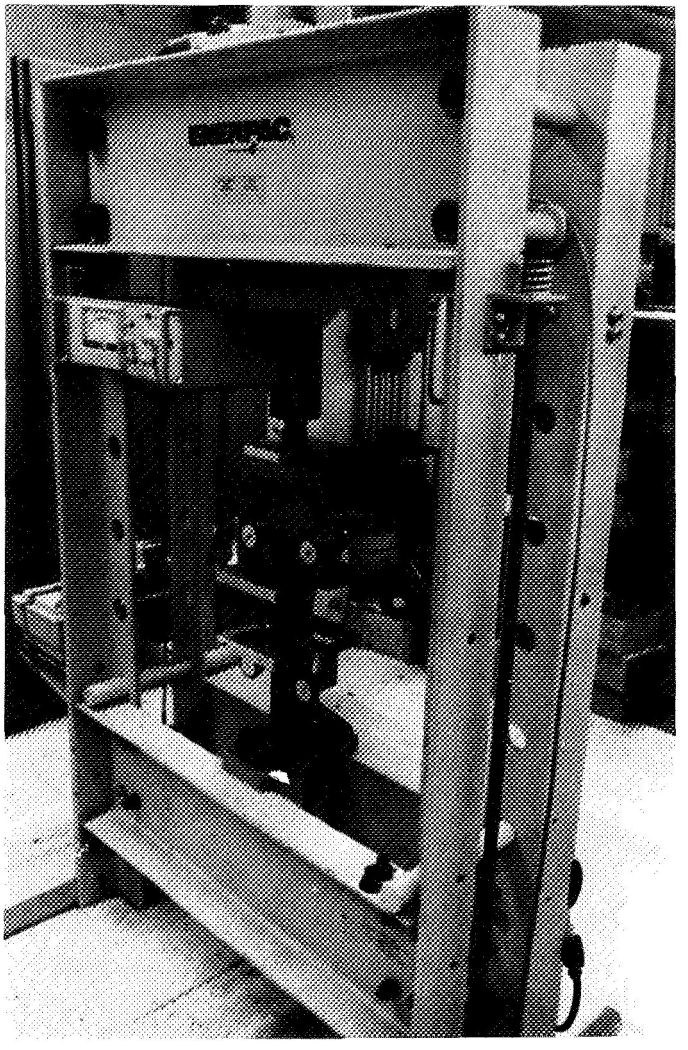

Fig. 1. Test stand with specimen in position

were mounted on the specimen for the duration of the test. All dial gauges were positioned to read positive when the specimen was tensioned and negative when the specimen was compressed. Readings were taken prior to loading, at 15-min increments for a total of 60 min., and at unloading. This procedure was repeated for reverse loading and continued for the duration of the test. Initial loadings always tensioned the specimen. Complete tests included five tension loadings of 1-h duration each and five compression loadings of 1-h duration each for a total of 10 h per test. Test loads were generated and maintained manually with a hydraulic hand pump. Temperature fluctuations never exceeded 4°F.

4. Results and Discussion

To compare the effect of specimen faying surfaces coating and bolt-type to slip displacement, an averaging procedure was employed. Since an individual test consisted of 51 readings, a point-by-point comparison of the value is almost impossible. Therefore, average values were calculated for each hour, even though slight variations were evident due to displacement with respect to time, or other inherent variations due to gage performance and the accuracy employed in reading the dial indicators. A typical example of this is shown in Fig. 2, which shows the results of three different tests averaged out. In general, the test results show no significant difference in slip displacement between hex and bearing-type bolts, when used with plain mill-scale-finish members. This is also true for the A325 and A490 strength levels of each type of bolts.

Inorganic-zinc-coated specimens were analyzed and are shown in Fig. 3. It can be seen in this case that bolt type does have an influence on slip-displacement behavior. With A325 bolts, the effect of bolt-type is not so pronounced, as slip displacements are somewhat the same until a net section stress of 17 psi is achieved. Beyond this point, the ability of the hex bolt to resist slip displacement is impaired, and a significant difference exists between it and the bearing bolt. With inorganic-coated specimens, at the same test loading, the slip displacement for both A490 hex and bearing bolts was found to be greater than for the A325 bolts. The net sectional stress of the A490 connection is lower than that of the A325 connection, at a given load level; the bolt shear stresses are identical. The only variables which could possibly explain the greater A490 joint slip over the A325 joint is

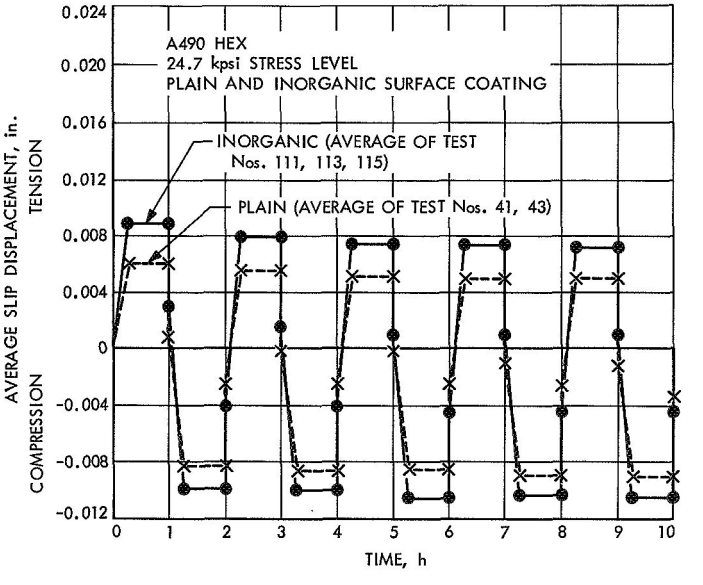

Fig. 2. Average hourly slip displacement versus time

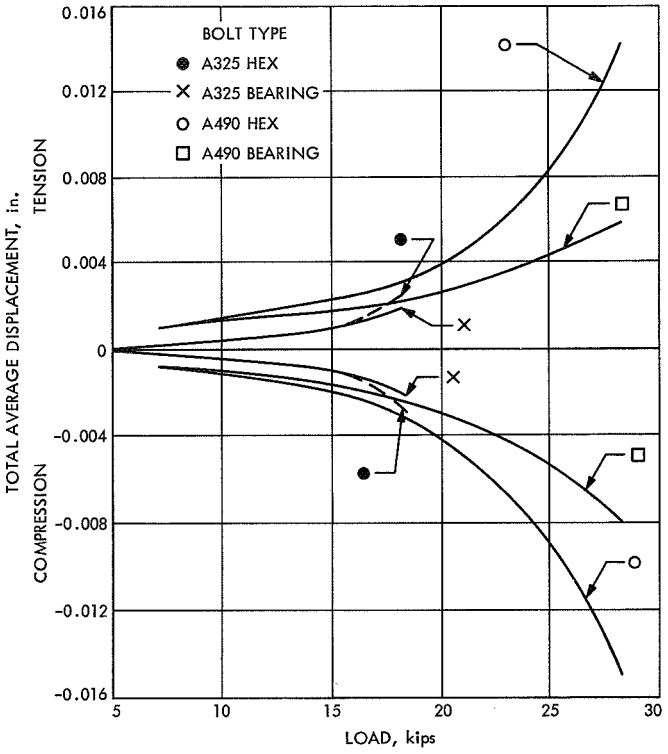

Fig. 3. Load versus average total slip displacement for inorganic-zinc-paint-coated specimens for different bolt types

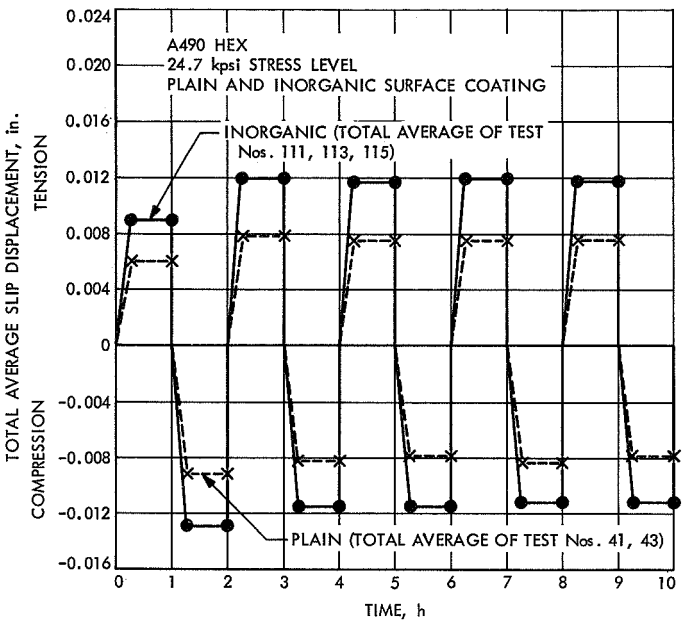

Fig. 4. Total average hourly slip displacement versus time

narrowed to those of bolt preload and the effect of the inorganic coating itself.

A490 bolts with inorganic-coated specimens demonstrate that bolt type (hex versus bearing) does have a pronounced effect on slip displacement, as shown in Fig. 3.

The A490 hex bolt allowed over 100% greater slip (at 100% design allowable) than the A490 bearing bolt. Therefore, it can be concluded that, however detrimental the effect of the inorganic coating may be with hex bolts, this can be negated through the use of bearing bolts with the same strength level.

The effect which inorganic faying surfaces coating has on joint slip displacement is illustrated by the behavior of A490 hex bolts as shown in Fig. 4. Slip displacement of inorganic-coated specimens is greater than those with plain faying surfaces at all test loads. At the lowest load level of 7.1 kips, or 25% of the design allowable, the inorganic-coated specimens averaged 0.004 and 0.003 in. greater slip displacement in tension and compression, respectively, than the plain mill-scale specimens.

At the highest scheduled test loading of 24.7 kips, or 87½% of design allowable, inorganic-coated specimens averaged 0.004 in. greater slip in tension, and 0.003 in. greater slip in compression, than the plain mill-scale specimens. At all loads, inorganic specimens averaged 0.002 in. greater slip in tension and compression than mill-scale specimens.

Although the net section stresses for all A490 connections as compared to A325 connections, at a given test load, were 32% lower, and the bolt shear stresses were identical, A490 connections with inorganic zinc-paint faying surfaces had greater slip displacements than A325 connections. This behavior could be due to the greater clamping pressures induced by the A490 bolts with respect to the A325 bolts (A490 bolts have 20% greater clamping pressure than A325 bolts). This increased clamping pressure apparently causes a premature microscope physical beakdown in inorganic-zinc coating. This breakdown in combination with the abrading action of the stress reversal results in a loss of bolt elongation, which leads to a loss in the original bolt clamping pressure and, consequently, a reduction in the resistance to slip displacement.

Spot checks of the coating indicate an average coating thickness of 4 mils (0.004 in.). The normal grip length, including washers for A490 bolts, was approximately one diameter, which is ¾ in. The A490 bolt elongation with

approximately the same grip is 0.005 in. when properly loaded. The initial tensioning of the bolts will cause some degree of coating compression. However, the combining effect of short bolt grips (low length-to-diameter ratio), thick relatively soft inorganic zinc painting coating, and the abrading action of stress reversal will cause a significant loss in bolt tension.

The above behavior may be true only for connection with relatively low bolt-length-to-diameter ratio. Thicker connections (larger length-to-diameter ratio) may not experience this phenomenon. Because of increased bolt elongation, due to longer grip length, (with identical coatings thicknesses) these connections would be less sensitive to losses in bolt elongation due to coating breakdown and may provide improved slip resistance.

5. Summary and Conclusions

The principal purpose of the research was to determine which design parameter and stress level would warrant use of inorganic zinc-painted coatings on specimens undergoing low-cycle low-load complete-stress reversals. In addition, part of the research program was to confirm previous stress-reversal studies concerning the effect of load level and type of fastener. The conclusions which were drawn from this research program follow:

(1) Slip displacement under complete stress reversal is a function of both applied external load and bolt shear stress. Slip behavior is not directly related to net sectional stresses.

(2) The effect which inorganic zinc paint faying surface coating has on joint slip displacement (all slip displacement refers to average total slip displacements) is illustrated by the behavior of A490 hex head structural bolts. Slip displacement is considerably greater than plain faying-surface specimens at all test loads. At lowest load levels (7.1 kips, 25% of design allowable), inorganic-coated specimens averaged 0.0004 in. greater slip than plain faying surfaces. At the highest scheduled test loading (24.7 kips, 87½% of design allowable) inorganic-coated specimens averaged 0.004 in. greater slip than plain faying surface specimens. Overall, inorganic coating averaged, at all loadings, 0.002 in. greater slip displacement than plain surface specimens.

(3) A significant fact resulting from the program is illustrated by the ability of the high-strength bearing bolt to negate the effects of faying surface coatings. Test results indicate that no difference can be attributed to faying surface coating when using either A325 or A490 high-strength bearing bolts.

(4) When comparing the effect of bolt types, relative to slip displacement, it is evident that no significant difference exists between A490 hex-head and A490 high-strength bearing bolts with plain faying-surface specimens. When the same comparison is made with inorganic-coated faying surface, the effect of the coating comes into play, and the hex structural bolts indicate inferior performance. This leads to the same conclusion stated previously; namely, that inorganic-coated faying surfaces permit greater slip displacements than plain surfaces.

(5) In respect to A325 strength level bolts, plain or inorganic coated specimens did not influence the slip displacement until 87½% of design allowable net section stress was achieved for coated specimens. Net section stress is greater than the aforementioned result in greater slip displacement for A325 hex bolts.

(6) Supplementary tests conducted at 100% design allowable on organic-coated specimens were comparable to previous tests done on research reported in SPS 37-52, Vol. II, pp. 92–97.

(7) A logical explanation for the greater slip displacement experienced by A490 connections with organic zinc paint faying surfaces than the A325 connections is two-fold: the A490 bolts have 20% greater bolt clamping pressure than A325 bolts, and this apparently causes premature microscopic physical breakdown of the inorganic-zinc coating; and this breakdown, in combination with the abrading action of the stress reversal results in a loss of bolt elongation and, hence, a loss of original bolt clamping pressure, and consequently increases slip displacement.

(8) Previous research (SPS 37-52, Vol. II) showed that faying surface coatings affected a joint's resistance to slip. From this previous research, a ranking of increased resistance to slip is as follows:

(a) Faying surfaces painted with red oxide primer give the least resistance to slip displacement.

(b) Zinc (hot-dipped galvanized) faying surfaces increase resistance to slip.

(c) Plain mill-scale faying surfaces further increase resistance.

(d) The most resistant were inorganic-zinc-painted faying surfaces.

This ranking of joint resistance does not hold true when the joint is subjected to load reversals. These tests showed different results when the specimens were loaded at 100% of design allowable stresses (20,000 psi) and 88% allowable design stress (17,000 psi). At these stress levels the inorganic zinc coating broke down and showed a greater slip than that of the mill-scale faying surface.

For the 210-ft deep space tracking antenna, where the stress levels generally run from 4,000 to 12,000 psi, the inorganic zinc silicate coating will not cause excessive slip under these low-level stress reversals. For stress levels of these magnitudes, the inorganic zinc silicate paint still affords an acceptable coating. However, the thickness of the inorganic zinc coating should be controlled in the area of the faying surface and should not exceed a thickness of 4 mils, and this coating should not be employed in any area subjected to stress reversal which could exceed the 17,000-psi stress level.

D. Switched-Carrier Experiments, *R. B. Kolbly*

The DSIF has a requirement, in support of the *Viking* mission, for simultaneous transmission of two carriers from one antenna. These carriers would be separated by approximately 5 MHz and carry ranging modulation. The power level required is a minimum of 40 kW in each carrier and its associated sidebands. The 400-kW transmitter can supply this easily if excitation is supplied at the two frequencies, but past experience and test data have shown that intermodulation products in the receiver passband well above threshold are generated by this approach. These products are generated whenever two carriers exist in the nonlinear klystron; there is even evidence that they may be generated in the waveguide equipment or the antenna structure.

If the excitation could be switched, so that the klystron and antenna see only one carrier at a time, these products would not be generated. Such an approach has been proposed by M. Easterling and the Goldstone Development Support Group of the RF Systems Development Section has started an experiment to determine the feasibility of this method.

The basic idea is to time-share the klystron between the two carriers by switching back and forth between them. If the switching is arranged so that each carrier is transmitted 50% of the time, each carrier will have 25% of the power and the other 50% of the power will be in the sidebands about each carrier at the odd harmonics of the switching frequency. If the switching frequency is chosen to be high compared to the bandwidth of any tracking loops and high compared to the command data rate, but low compared to the ranging modulation and different from the command subcarrier, there will be no interference due to the switching sidebands. The problem of choosing a switching rate relative to the command subcarrier is similar to the problem of choosing two noninterfering telemetry subcarriers.

There is a possible problem during the acquisition of a carrier in that the carrier tracking loop in the spacecraft might lock to a switching sideband. This is very unlikely if any reasonable switching frequency is used. If it should be considered to be of concern, the problem could be avoided by switching with a pseudonoise (PN) sequence which would spread the spectrum of the switching sidebands and leave no strong signal for a possible spurious lock. The spread spectrum might cause some degradation of the tracking loop performance, however, by putting some of the sideband energy into the loop bandwidth. This suggests that a proper strategy might be to use PN switching during acquisition and square-wave switching during tracking. Changing from one to the other would have no effect on the signal being tracked by either spacecraft.

The proposed approach has a 50% efficiency independent of the modulation on either carrier. Thus, it would provide two 100-kW carriers from the 400-kW transmitter or two 5-kW carriers from a 20-kW transmitter. The equipment in Fig. 1 is being utilized to investigate the feasibility of the above approach. The diplexer assembly is installed in such a manner that

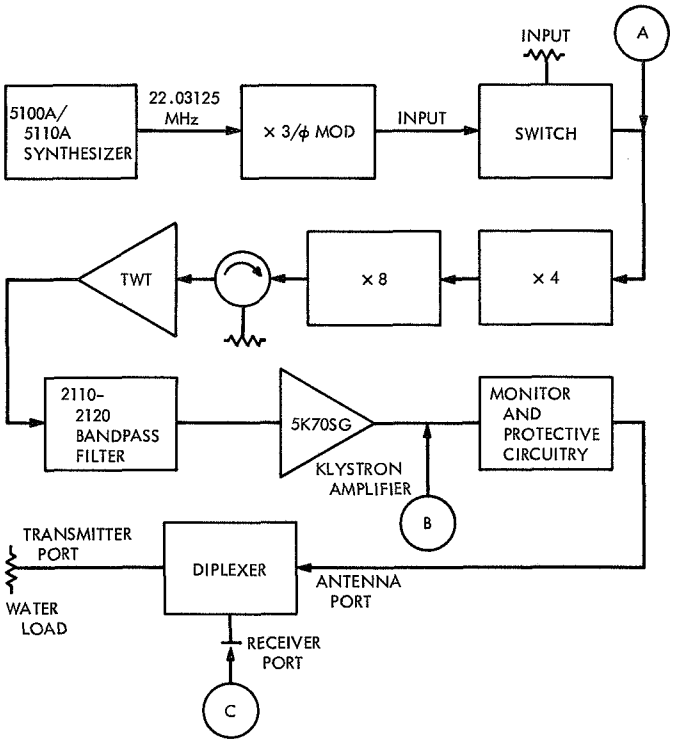

Fig. 1. Switched-carrier test configuration

there is very low loss (less than 1 dB) between the output of the klystron and the detector in the receiver (2290–2300 MHz) band. Since we will be measuring very high order sidebands (i.e., when switching 2115 MHz at 500 kHz, the 360th sideband falls at 2295 MHz), the 500-kHz switching frequency is derived from a stable source, the same synthesizer used to furnish the 22.03125 MHz for the exciter.

At this time, experiments are being run using one carrier switched on and off at a 500-kHz rate. Since the 500 kHz is coherent with the exciter frequency, we are able to determine the source of a particular sideband or spurious product. By using one frequency rather than two, we are concerned with only one-half of the total spectrum, simplifying the analysis of data. Since we can treat each carrier as being keyed on and off, we will suffer no loss of data by this approach. Also, the use of the 2115.000000-MHz carrier and the 500.000-kHz switch rate allows modulation sidebands to be separated from any other spurious products.

A diode switch has been built to perform the 66-MHz switching function. Figure 2 illustrates the final configuration of the switch. The diode switch is driven with a biphase 0 to −16-V 500-kHz square wave which is supplied from modified 3C S-PAC digital logic cards.

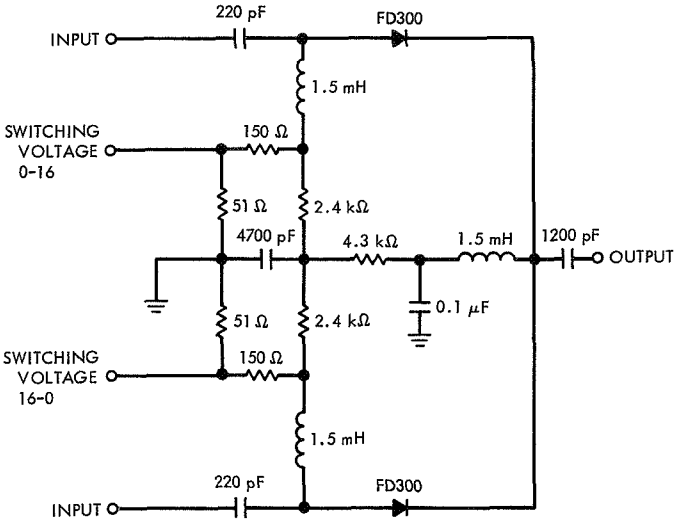

Fig. 2. Diode switch schematic

Figure 3 is the spectrum measured at point A in Fig. 1. This indicates that the diode switch is performing as predicted. Figure 4 is the spectrum at the output of the klystron amplifier. The sidebands have been filtered by several bandwidth limited items at this point, including the klystron amplifier. It will be noted that because the klystron is operating in a saturated mode the rise time of the output pulses is sharpened.

This investigation will continue with the following experiments:

(1) Investigation of spurious and modulation products in the output of the klystron in the DSIF receiver band (2290–2300 MHz). This will be done with a sensitive phase-lock receiver and a low-noise preamplifier.

(2) Investigation of spurious and modulation products close to the transmitted carriers.

(3) Measurement of system temperature in a standard DSIF diplex configuration with switching.

The results of these tests and the feasibility of using this system to support dual carrier commitments will be examined.

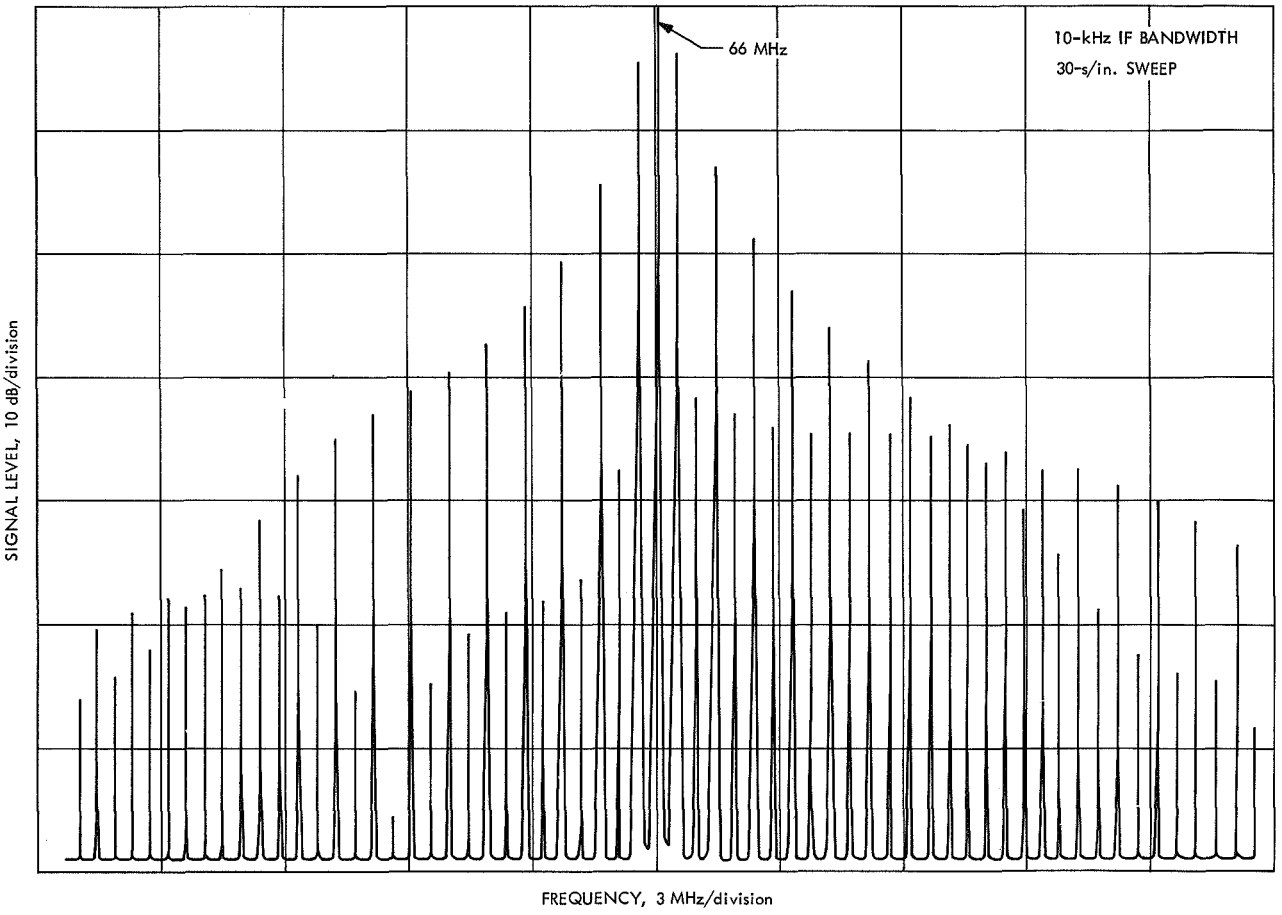

Fig. 3. Spectrum at output of diode switch

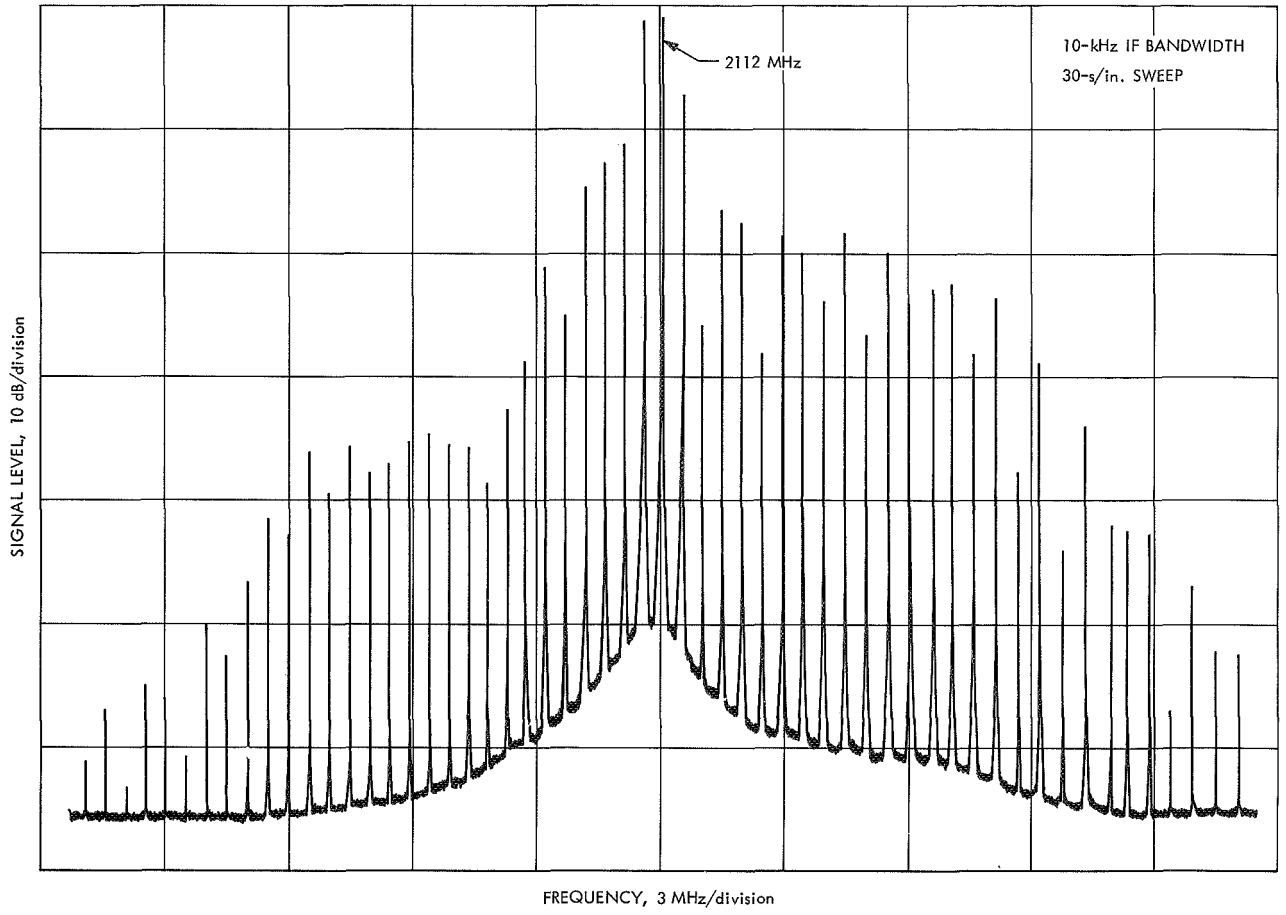

Fig. 4. Spectrum at output of klystron amplifier

E. DSS 13 Operations, *E. B. Jackson*

During the period June 16 through August 15, 1970, the major activities at DSS 13 included a special clock synchronization experiment, routine pulsar observations for 24 h each week, cooperative planetary radar activities and continued development of the ephemeris update tracking program (SPS 37-60, Vol. II, pp. 70–71). Installation of the Model IV receiver/exciter was completed and long-term testing begun; installation of the 100-kW, 2115-MHz transmitter was also completed.

Continuing with the clock synchronization experiment which was begun on June 1, 1970, daily transmissions were made to DSSs 14, 41, 42, 51, and 62, the National Bureau of Standards (NBS) and the U.S. Naval Observatory (USNO). This experiment is to determine the resolution and accuracy possible with the existing system, and explore the reliability of both the transmitting and receiving stations with regard to capability to support daily long-term operation.

The experiment worked very well, and some system weaknesses were uncovered; for example, the narrowband receiving filter had a tendency to drift in center frequency. Additionally, it was shown that the system resolution is such that the effects of the Moon's topography cause a periodic variation in the timing of the received data. The experiment was completed on July 31, 1970, and transmissions continue only to DSS 14, the NBS, and the USNO on a regularly scheduled basis.

An additional cooperative experiment was performed with DSS 14 and the Haystack Facility of the Massachusetts Institute of Technology. This was an effort to make precision ranging measurements of the planet Mercury when it was in appropriate position with respect to the Sun. Although good data were received from the test targets (Venus and the Moon), data from Mercury were too noisy to provide the precision range points desired. The amount of signal returned from Mercury, at 7840 MHz, using a 10-μs range gate, is insufficient to provide the required signal-to-noise ratio.

A continuing program of making once-weekly precision range measurements on the planet Venus was begun during the last week in July. Using a 10-μs range gate, good data have been collected for three weeks. This experiment will continue through the end of 1970.

The ephemeris update tracking program (scan and correct, using receiver–SCOUR) has been developed to the point where successful automatic tracking of radio stars and spacecraft has been demonstrated. In this scheme, an output from the receiver proportional to the received signal is monitored by a digital computer while the computer commands the antenna to perform a scan. The variations in the received signal level while scanning are used by the computer to develop error signals to drive the antenna until the radio star or the spacecraft are maintained in the center of the antenna beam. Preliminary indications are that the signal degradation is quite small, but further testing and optimization is underway.

Long-term testing of the Model IV receiver/exciter has commenced. This receiver/exciter, constructed primarily of integrated and hybrid circuits, has real-time digital-computer-controlled first local oscillator frequency so that automatic acquisition of a spacecraft can be effected. Several successful spacecraft tracks have already been accomplished and more will be performed as the various operational parameters (sweep rate, phase lock loop bandwidth, sweep direction, etc.) undergo optimization. Spacecraft tracked to date include *Mariners VI* and *VII* and *Pioneers VIII* and *IX*. Observed signal levels vary from −168.8 dBm (*Pioneer VIII*) to −173.2 dBm (*Pioneer IX*).